TIP-TILT-PISTON ACTUATORS FOR HIGH FILL-FACTOR MICROMIRROR ARRAYS

Veljko Milanović, Gabriel A. Matus, Daniel T. McCormick

Adriatic Research Institute
828 San Pablo Ave., Suite 115E, Berkeley, CA 94706
veljko@adriaticresearch.org

ABSTRACT

Tip-tilt-piston actuators for optical phased arrays with large deflection angle, large piston range, and fast update rates are demonstrated. The devices include bonded low-inertia micromirrors on top of actuators aimed to achieve >96% fill-factor arrays. The gimbal-less design methodology enables scaling devices down to a few 100 μm to allow future implementation of large arrays with <100 μsec update. Several different design architectures have been successfully fabricated and tested as individual devices, and as a 2x2 element array. Devices with square layouts are demonstrated with 800 μm down to 400 μm on a side. In each case the devices consist of 4 vertical combdrive rotators connected by 2 degree-of-freedom (DoF) linkages to a central stage. Each actuator can rotate bi-directionally to raise or lower its linkage, giving the stage the required 3 DoF. The stage is used as a platform for bonding of a thin, low-inertia mirror plate which then completely covers the actuator. A representative high field-factor actuator of 500 μm x 500 μm dimensions achieves optical deflection angles beyond -20° to 20° for both axes and greater than -12 μm to 12 μm pistoning, at <80V actuation. In comparison, a larger low field-factor device with a 600 µm diameter integrated micromirror is also demonstrated which utilizes 3 bi-directional actuators radially offset by 120° to achieve tip-tilt-piston actuation with -10° to 10° deflection in all axes and -30 µm to 30 µm pistoning.

I. INTRODUCTION

A. Background

Various optical applications require large adaptive apertures with rapid reconfiguration rates. Even in the case of simple beam steering, increasing the mirror size results in significantly increased response times due to increased inertia. Therefore, it is desirable to replace large mirrors with phased arrays of smaller micromirrors. This offers several advantages such as significantly higher steering speeds and remarkably improved optical and mechanical properties. Past efforts have emphasized the need for such arrays ([1],[2]) but have not achieved all three degrees of freedom (3-DoF, tip-tilt-piston,) nor sufficiently high speeds of operation. Namely, if such 3-DoF device-phased arrays were available, it would enable more sophisticated optical beam shaping, multiple-beam steering, and a variety of general adaptive optics application.

In Figure 1a, four tip-tilt-piston actuators are arranged in a 2x2 array with minimal spacing between the actuators to achieve high fill-factor of the reflecting surfaces in Figure 1b. Each actuator in Figure 1a is rectangularly arranged with 400 µm on each side, and its central stage can be actuated to tip-tilt-piston, as will be discussed in more detail in Sec. II. After transfer and bonding of separately fabricated single-crystal silicon mirrors (Figure 1b,) the devices can be used independently, as four scanners, or together, as one larger (800 x 800 µm) aperture, etc. The elements in Figure 1b are not functional as it is impossible to reach the actuating electrodes beneath the micromirrors, but were used for bonding demonstration purposes. In the future, larger arrays with perhaps 1000s of elements could therefore have remarkable impact in numerous photonics applications.

B. Two-axis scanners and the gimbal-less approach

Recently, we have developed independently and linearly controllable vertical comb drives using only a single SOI device

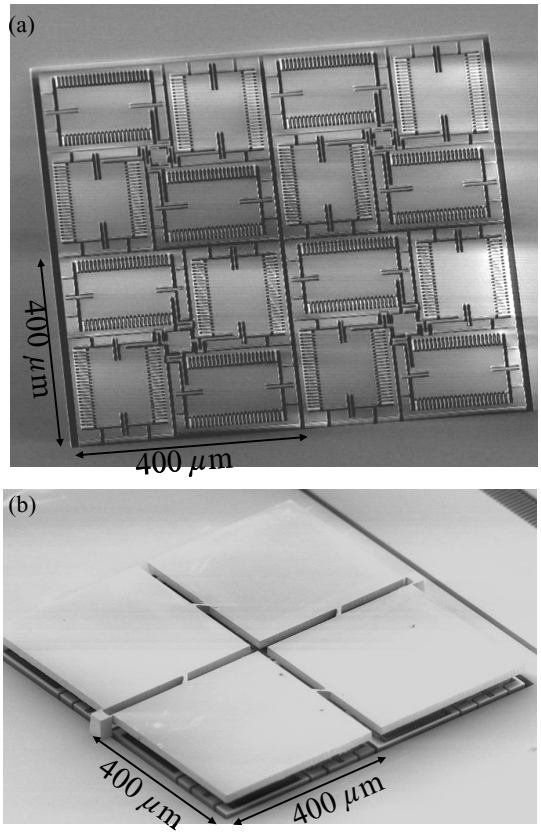

Figure 1. SEM micrographs of a fabricated 2x2 element array of high aspect-ratio tip-tilt-piston actuators: (a) actuators as fabricated in the SOI device layer and before micromirror bonding, and (b) after bonding of a 2x2 array of low-inertia micromirrors, still tethered together for simultaneous transfer and alignment.

layer, thereby realizing monolithic structures with isolated actuators [3]. These devices are fabricated in the Multilevel-beam SOI-MEMS process [4]. Our goal was primarily to expand their use to two-axis micromirror scanning applications, while maintaining the high-speed operation possible in the one-axis devices and minimizing cross-coupling between axis. An additional goal has been to achieve devices with tip-tilt-piston capability, i.e. 3 DoF actuation, for phased array applications. Such applications have an additional requirement that the devices should easily scale down to small dimensions.

The most common method of implementing two-axis (two degrees of freedom, 2DoF) rotation has been through the use of a gimbaled structure [5],[6],[7], although packaging-based methods with one-axis scanners are utilized as well. However, to implement 2DoF gimbaled micromirror without cross-talk between driving voltages, electrical isolation of the mechanical coupling linkages is required. Backfilling of isolation trenches by an additional deposition layer followed by a chemical mechanical polishing (CMP) step has been used to achieve the electrically isolated mechanical coupling [7],[8]. The additional deposition and CMP steps significantly increase both the complexity and cost of the fabrication process. Typically, gimbaled designs result in non-symmetric and relatively slower achievable response frequencies

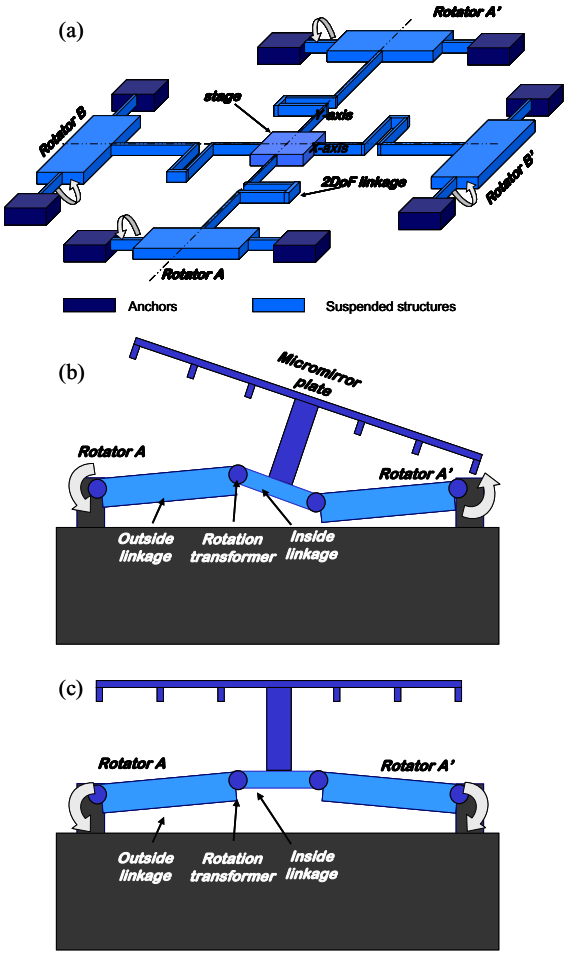

Figure 2. Gimbal-less tip-tilt-piston scanner's operation: (a) 4 bi-directional rotators, here shown just as torsion beams working in pairs to provide each of two axes of rotation. (b) cross-section A-A' example of x-axis actuation, actuator A and A' both turn in the same direction, giving micromirror rotation with a virtual axis at center. (c) cross-section A-A' in an example where both actuators A and A' lift the central stage in common-mode, achieving pistoning.

between the two axes due to the gimbal's slower outer axis. Our approach for high-speed two-axis scanning in [9] was based on pre-engaged vertical combdrives in SOI and gimbal-less design.

In that methodology, we utilize the previously demonstrated one-axis vertical combdrive-based rotation actuators [3], which are discussed in more detail below. These rotators are then combined utilizing mechanical linkages that allow 2DoF of rotation for a central micromirror in differential operation (Figure 2b,) and pistoning in common-mode operation (Figure 2c.)

II. Background and Device Principles

A. One-axis rotators

The basic building block for our two-axis and tip-tilt-piston scanners is a one-axis rotator. Due to the capabilities of the Multilevel-beam SOI-MEMS process [4] to provide isolated combdrives with different actuation force directions, a designer can choose optimized combdrives in a given application. The four types of actuators we most commonly use are shown in the micrographs of three fabricated devices in Figure 3. Figure 4 depicts their cross-sections.

1) The first type of actuator in Figure 4(i) utilizes Down combs and Up combs on opposing sides of the axis of rotation to achieve uni-directional pure rotation. During counter-clockwise rotation, overlap area increases on both sides, increasing capacitance. As

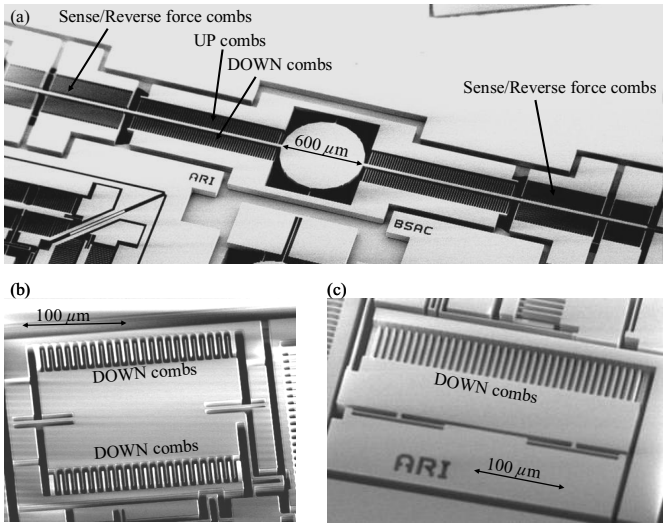

Figure 3. Uni- and Bi-directional one-axis rotators which are the main building blocks of two-axis scanners and tip-tilt-piston actuators: (a) one-axis pure-rotation with integrated and isolated sense capacitance/reverse force actuation fingers, (b) bi-directional DOWN rotation actuator, and (c) uni-directional DOWN actuator.

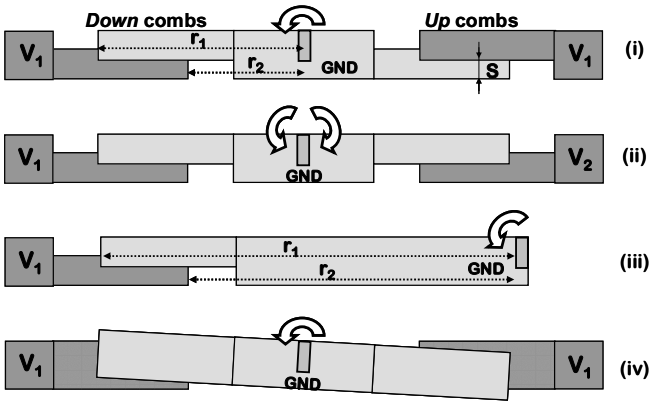

Figure 4. Schematic cross-sections of SOI device layer arranged to achieve 4 distinct modes of operation, such as bi-directional rotation and pistoning.

discussed in [9], it is difficult to represent the desired quantity $dA/d\theta$ in closed-form. However it can be estimated to within ~5% by a simple and useful expression:

$$dA/d\theta \approx 0.5 \cdot \left(r_1^2 - r_2^2\right), \tag{1}$$

where r_1 is the distance of the rotor finger tip from the rotation axis, and r_2 is the distance of the stator finger tip from the rotation axis (Figure 4(i)). Because the fingers are initially pre-engaged such that linear operation from onset can be assumed, we can make a further approximation, neglecting fringing field effects:

$$\frac{dC}{d\theta} \approx 2\frac{\varepsilon_0}{g} \cdot \frac{dA}{d\theta} \approx \frac{\varepsilon_0}{g}\left(r_1^2 - r_2^2\right), \tag{2}$$

where ε_0 is air permittivity and g is the gap distance between combfingers. The factor 2 in (2) comes from the fact that a combfinger has two sides which contribute to the capacitance.

We then plug (2) into the well-known electrostatic torque equation,

$$\tau = N\frac{1}{2} \cdot \frac{dC}{d\theta} \cdot V^2 \approx \frac{N \cdot \varepsilon_0}{2g}\left(r_1^2 - r_2^2\right) \cdot V^2, \tag{3}$$

accounting for N combfingers in an actuator. Rotation eventually causes the fingertips to disengage. As the combfinger tips pass

through, the rate $dA/d\theta$ is no longer constant and drive no longer follows the voltage squared law. Combdrive stroke and combfinger length are the main parameters that determine this disengagement angle. The simplest approximation for the maximum angle is thus simply $\theta_{max\_lin} \approx tan^{-1}(S/r_1)$ (Figure 4 (i)). The drive will continue to rotate past θ_{max_lin}, but the rate $dA/d\theta$ decreases and eventually changes sign, i.e. the area begins to decrease and the vertical comb drive loses drive ability. Therefore, the approximations in (1)-(3) are only valid in the range $0° < \theta < \theta_{max\_lin}$.

2) The type of actuator in Figure 4(ii) utilizes Down combs on both sides, resulting in bi-directional rotation when one side is activated at a time, though with some unwanted lateral and vertical motion. With both sides activated, it gives pistoning Down motion. The same approximations from the case 1) above apply, except that only one half of the total number of combfingers actuate in either direction.

3) The third type of actuator in Figure 4(iii) utilizes only Down combs to provide uni-directional rotation. The trade off is that, given the same space considerations as in (ii) and (i), the torque arm can be twice as long giving four times the torque.

4) The fourth type of actuator in Figure 4(iv) utilizes full thickness, High beams for combfingers which are perfectly overlapping at $\theta=0$. However, as θ increases beyond zero to either direction, applying voltage to this actuator gives reverse-force, i.e. force to return to $\theta=0$. The 2nd purpose for such combdrives is to utilize them as isolated sets of capacitance sense fingers, as in the device of Figure 3a. In that case, during the device operation, monitoring the capacitance on those combdrives provides position feedback for closed-loop feedback control which is described in [14].

Equations governing these types of combfingers follow from above, approximating the area change and therefore torque as:

$$\tau \approx -\frac{N \cdot \varepsilon_0}{2g} \cdot \left(r_1^2 - r_2^2\right) \cdot V^2. \qquad \theta \neq 0 \tag{4}$$

When used in capacitive sensing circuits such as [14], reference capacitors are fabricated on chip utilizing the same layout in order to insure matched capacitances.

B. Two-axis scanners with integrated micrormirrors

As mentioned above in Sec. I*B*, to achieve the goal of fast two-axis scanning, we combine multiple one-axis actuators positioned orthogonally, and utilize mechanical linkages to allow two-axes of rotation for a central micromirror, as first demonstrated in [9]. Two one-axis rotators are utilized for each axis of the overall two-axis scanner. For the *x*-axis, actuators A and A' are utilized, and for the *y*-axis, actuators B and B'. The actuators are attached to the mirror through a set of beams and a mechanical rotation transformer. The problem of combining one-axis actuators discussed above in Sec. II*A*, and allowing their operation to be mostly unaltered by the other axis' operation, is addressed as follows. Each linkage that connects an actuator to the central micromirror is actually designed to be a two degree of freedom (2 DoF) mechanical component which allows rotation via transformers, and allows de-coupling from the orthogonal axis via torsional compliance.

An important design feature is that the position of the mechanical rotation transformer in Figure 2b governs the mechanical rotation gain *G* between the micromirror's and actuator's rotation. Namely, since the actuator rotates about its axis, and the micromirror stage rotates about a virtual stationary axis (due to opposing actuations on either side in Figure 2b,) the angles relate as $\theta_{\text{mirror}} / \theta_{\text{act}} = G = d_2/d_1$. In that, d_2 is the length of the inside linkage from the transformer to the mirrors center, and d_1 is the length of the outside linkage from the actuator's axis to the

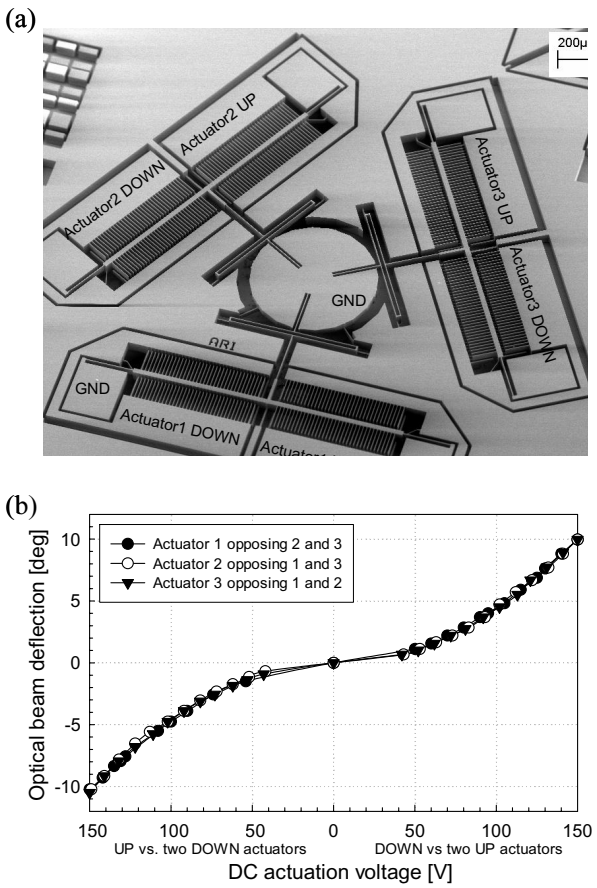

Figure 5. Large tip-tilt-piston "Triangle" device with integrated 600 µm diameter micromirror demonstrating the use of 3 bi-directional rotators arranged around the central stage for tip-tilt-piston operation (b) optical beam deflection measurement in 3 axes, with actuators working in differential modes (2 opposing 1) and (c) pistoning characterization with all actuators working in common mode (all three Up or all three Down).

transformer. This feature is very beneficial due to the following: the maximum angle of each rotator is given by combdrive dimensions as discussed in Sec. II*A* above, while the micromirror angle can be arbitrarily increased by using $G>1$. Moreover, proper design use of mechanical gain can significantly increase overall device speed as $G^{-1/2}$, because it allows increased finger length and torque while achieving same desired large angles of micromirror rotation.

By utilizing these principles and increasing the length of each rotator to obtain large torques and better stability, most recent devices with integrated 600 μm diameter micromirrors achieve >20° optical deflection while maintaining lowest resonances > 4.4 kHz.

C. Implications to Tip-Tilt-Piston array elements

In order to achieve the goal of large optical phased arrays with high fill factor (e.g. >96%,) and tip-tilt-piston actuation of each element, several significant issues have to be addressed and improved on the previous monolithic two-axis scanner work:

1) The actuators must be completely covered beneath the micromirror's reflecting plate for high fill-factor, therefore additional fabrication/packaging solutions are required. Some examples of previous work are given in [1],[5],[10]-[12]. We currently address this issue by separately fabricating low-inertia silicon micromirrors and transferring/bonding them into place on top of the provided actuators stages. This is described in Sec. III*C*.

2) The actuators must be designed in a way to provide independently controllable pistoning in addition to tip-tilt actuation,

for phase correction. As shown in Figure 2, this can be achieved if all rotators are bi-directional. In their common mode operation, pure pistoning is achieved, while in differential mode operation, tip- or tilt- rotation. We have demonstrated this concept in a large device with three bi-directional actuators arranged at 120 degree positions relative to each other (Figure 5a.) Measurements for the device are given in Figure 5b and Figure 5b. It was tested for three different axes. Namely, the device shown has 3 bi-directional actuators, such that any of the actuators can either actuate the linkages Up or Down, depending on which electrode is activated. For example, for testing of the actuator 1 axis in the positive angle direction, we actuate the actuator 1 Down while actuating actuators 2 and 3 Up. The actual axis of that rotation is parallel to actuator 1 shuttle, through the micromirrors center. The opposite arrangement results in a negative angle deflection. Analogous configurations were employed for each of the remaining axis. In the common-mode arrangement full-stroke pistoning actuation was measured from -30 μm to 30 μm.

3) The actuators must be reduced in size significantly to fit beneath a mirror with an edge dimension of less than 600 μm, while maintaining large torque and therefore high speed operation.

4) In an array of such elements, routing of signals to each element must be provided.

In the present work, we address issues 1) thru 3), demonstrate proposed actuator designs, and discuss results. The routing and packaging solutions for 4) are planned as future work.

III. DEVICE FABRICATION

A. Summary of Multilevel beam SOI-MEMS process layers

All of the actuators in this paper were fabricated using the multilevel beam SOI-MEMS process, described in detail in [4], which will be only briefly summarized here, as it applies to the array-element actuators.

The process requires three photolithography masks and three DRIE etches in order to achieve the desired 3-level beams as shown in Figure 6. In the process aimed at larger devices (e.g. Figures. 5 and 6) with significant vertical displacement during actuation, back-side etching is also required to provide large cavities for such movement. Those therefore require a total of four masks. For small array elements, that do not include a large integrated micromirror, back-side etching can be eliminated since there is no requirement for providing space for large vertical displacements and rotations. Therefore, as shown in Figure 6, three masks are used to DRIE etch into the device layer of an SOI wafer and achieve isolated sets of vertical combdrives with *UP* or *DOWN* actuation.

The first layer of photolithography is applied to the device wafer's backside prior to SOI wafer formation, which allows for the mask *Backup* to be etched into that wafer before SOI bonding. After the SOI bonding, grinding and polishing, the remaining two masks are applied on the front of the device layer and aligned to the pre-etched *Backup* mask in the SOI wafer. Two timed DRIE etches on the front side of the wafer complete the shaping of the device layer, resulting in four types of beams, *High*, *Upper*, *Lower* and *Middle*. *Upper* and *Lower* are approximately three fifths of the device layer thickness with an overlap of approximately one fifth, while *High* beams are of full device layer thickness. The resulting structures are high aspect ratio, fully monolithic single crystal silicon structures.

B. Design and fabrication of low-inertia micromirrors

Low inertia micromirrors are fabricated in a separate SOI wafer employing a 3-level selective DRIE process (Figure 8). The mirrors are realized from monolithic single crystal silicon and consist of a full-height pedestal, thinned mirror plate, and mid level trusses. The pedestal provides a bonding surface for attachment to

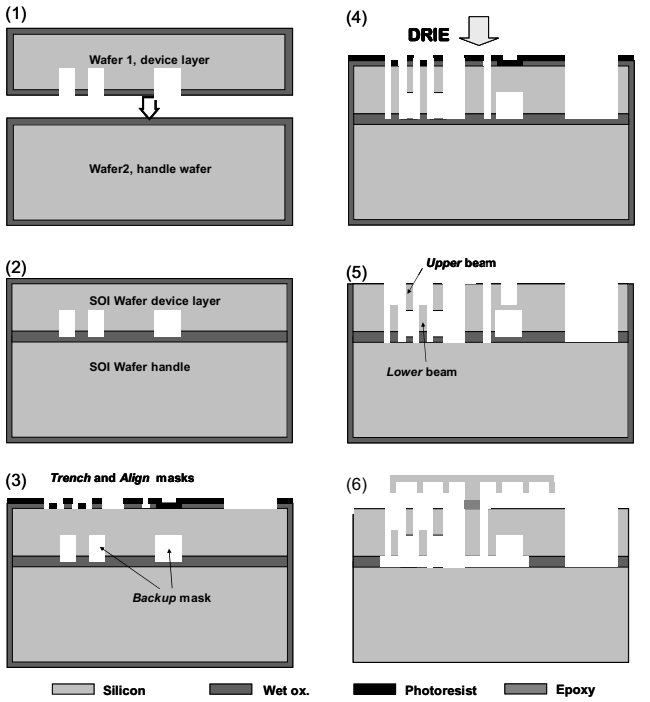

Figure 6. Schematic of the process steps to fabricate the high fill-factor devices with bonded mirrors in this work.

the designed receiving platform on the actuators; it also serves as a stand-off, providing separation between the mirror and actuator to allow sufficient rotation. Thinning of the mirror plate results in a significant reduction of the device's moment-of-inertia. Minimizing the inertia and mass of the structure allows higher resonant frequencies to be achieved without reducing the compliance of the actuation structure's suspension. The fabrication process also incorporates truss structures in order to provide a stiffening backbone for the thin mirror. Analytical and finite element models (FEM) of the device are employed to optimize the design of the mirror and truss structures in order to minimize the inertia as well as dynamic deformation of the mirror plate. Furthermore, FEM is utilized to avoid undesirable, excitable modes. The trusses are also designed to allow the thin mirror plates to be metalized with approximately 100 nm of aluminum with minimal warping and static deformation.

The fabrication of the low inertia micromirrors is initiated by growing a thick oxide layer (~2μm) on an SOI wafer with a device layer thickness equal to the desired thickness of the pedestal plus the mirror plate. The oxide layer is then patterned with three consecutive lithography steps and RIE oxide etches (Figure 8a). These etches define a multi-tiered oxide hard-mask for the subsequent DRIE silicon etches. During the first DRIE step only the silicon that will be etched down to the buried oxide layer is exposed; the depth of this trench etch is greater than the desired thickness of the mirror plate. A blanket RIE oxide etch then completely removes the thinnest oxide hard-mask, while thinning the remaining oxide masks. The second DRIE determines the thickness of the trusses by recessing the mirror plate to the desired depth. A second oxide etch removes the truss hard-mask. The final DRIE step lowers the parimeter trench, truss beams and mirror plate simultaneously; after the buried oxide layer is reached at the bottom of the outer trench the etch is terminated when the desired mirror thickness is achieved (Figure 8b). Finally the mirrors are released in concentrated hydro-fluoric acid (HF) (Figure 8c).

In the present work the thickness of the pedestal is 50μm, the trusses are 15μm and the mirror thicknesses is 2μm. SEMs of example fabricated mirror structures are presented in Figure 9.

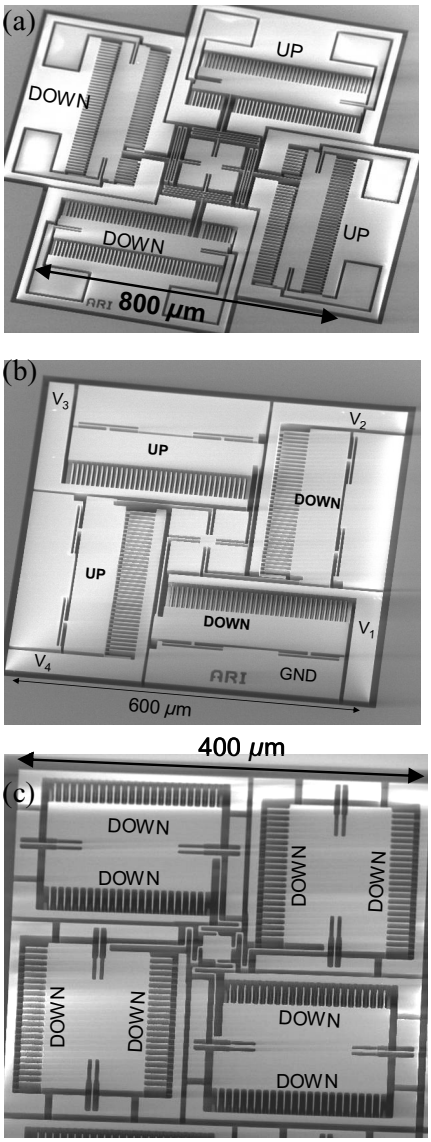

Figure 7. a) 0.8 mm x 0.8 mm (HFF800) device with large pads for prototype testing, four one-directional rotators are arranged around a central stage. (b) 0.6 mm x 0.6 mm (HFF600) device with different (L-shaped) type of 2DoF linkages between one-sided rotators and the central pedestal, and (c) a 0.4 mm x 0.4 mm device (HFF400) showing four bi-directional rotators around the central pedestal. HFF500 devices (0.5 mm x 0.5 mm) were also fabricated as a scaled version of the HFF400 devices, with same layout.

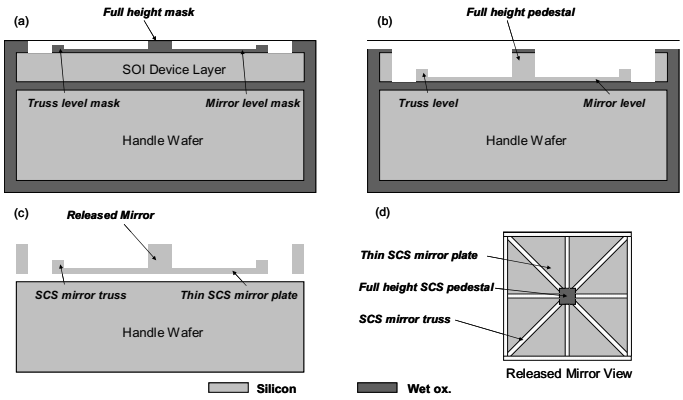

Figure 8. Schematic fabrication process steps for the three-level low-inertia micromirrors in a separate SOI wafer.

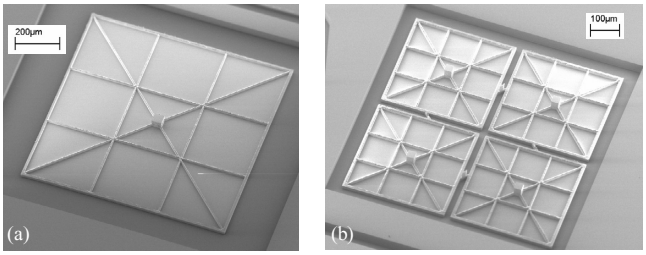

Figure 9. Fabricated low-inertial mirrors before release from the SOI wafer. Three thicknesses are visible, the thin mirror plate, thicker trusses for robust and flat support and the tall pedestal.

C. Transfer and bonding of low-inertia micromirrors onto actuators

The low inertia micromirrors must be attached to the actuators, which are realized on a separate wafer. Transfer and bonding of individual thinned micromirrors onto the actuators was achieved using custom fabricated "capillary pickup fingers," [13] which hold the micromirror from the top, flat side. In this work a small quantity of optical epoxy is applied to the actuator's pedestal platform using a micromanipulator and a simple tungsten probe tip. The mirror is held by the capillary pickup fingers, on a separate micromanipulator. Following optical alignment of the mirror and actuator while viewing on the microscope, contact is made between the pedestal and platform. The surface forces tend to bring the pedestal into perfectly flat alignment with the stage as soon as contact is made, and the capillary pickup fingers then release the mirror. Finally the epoxy is exposed to ultra-violet light followed by a curing step in a 125°C oven.

Batch bonding and alignment of multiple mirrors for large-scale, high fill-factor arrays is an on-going effort, with the 2x2 array in Fig. 1c demonstrated to date.

IV. CHARACTERIZATION AND CONCLUSIONS

A variety of designs of high fill-factor (HFF) actuators have been designed and fabricated, as shown in Figure 7, in all cases utilizing 4 one-directional actuators arranged around the central mirror. Several devices of each kind were tested. By electrically activating the proper pair of electrodes, different actuation modes have been independently demonstrated. By observing the deflection of a laser beam against a metric wall, we measured the rotations of both the micromirror as well as the actuators which reflect a small portion of the beam (the laser beam covers the entire device.) In that way we are able to verify the overall performance as well as the mechanical gain between the center stage and actuator rotation. For pistoning mode characterization we utilized a Laser Doppler Velocimeter.

Large numbers of devices have been successfully tested as fabricated on a probe station, with a summary of the results is given in Table 1. The smallest device (400 μm on a side) measured >20° of optical deflection in both axes and >64 kHz and >30 kHz resonant frequency in rotation and pistoning, respectively, prior to mirror bonding. A representative high field-factor actuator of 500 μm x 500 μm dimensions (HFF500) achieves optical deflection angles beyond -20° to 20° for both axes and greater than -12 μm to 12 μm pistoning, at <80V actuation, as summarized in Figure 10.

It is also important to note, as shown in Figure 11 for a 500 μm actuator and an 800 μm actuator, that for devices with bonded micromirrors the quality factor (Q) (which is extracted from the measured step response) decreases significantly. The Q of the 800 μm device is reduced from ~50 to 2.50 with a bonded micromirror, and for a 500 μm device the final Q was 1.46. This reduction in Q is the result of increased damping due to the effects of surrounding air, and is highly desirable for faster settling time operation. A settling time of ~ 2 ms in open loop actuation was extracted from the plots.

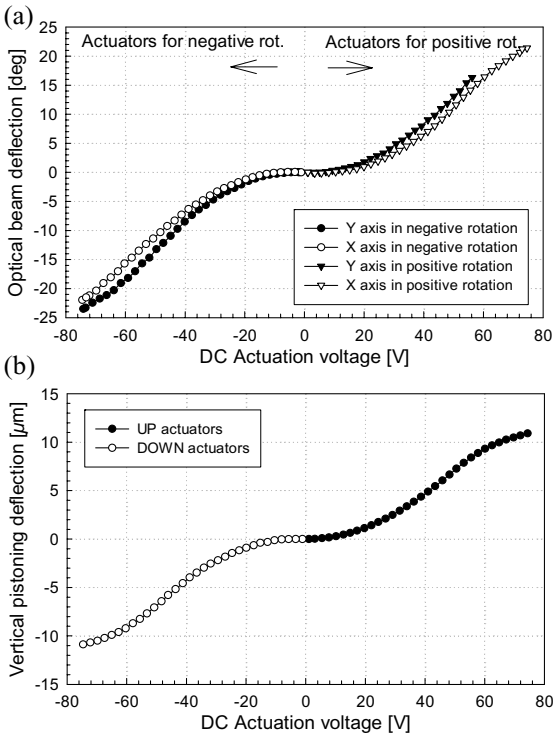

Figure 10. Measured HFF500 actuator in (a) bi-directional rotation for both axes, and (c) bi-directional pistoning actuation..

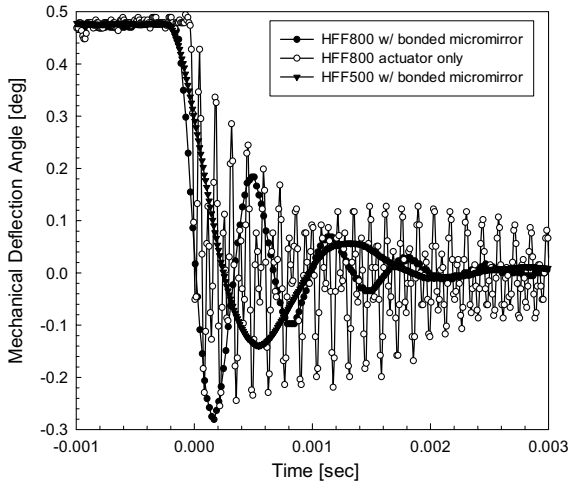

Figure 11. Measured comparison of an HFF800 device step response before and after mirror bonding, showing an approximate 10x reduction in resonant frequency of the ringing, and similarly a very significant decrease of the quality factor from ~ 50 to 2.5 due to the effects of the air surrounding the micromirror. Superimposed is the step response for the HFF500 device with the bonded micromirror with Q of 1.46.

The present methodology is very promising for high speed and large static deflection 2D scanning applications as well as high fill factor arrays of small mirrors with tip-tilt piston capability for each individual element. It enables the designer to significantly optimize independent components and achieve desired overall performance. The actuators and mechanical linkages allow static two-axis rotation of for micromirrors without need for gimbals, or other specialized isolation methodology. The design presented

	X-axis scan optical °	Y-axis scan optical °	Res. freq no mirror [Hz]	Res. freq W/ mirror [Hz]
Triangle	-10 to 10	-10 to 10	n/a	4096
HFF800	0 to 12.5	0 to 14.5	22727	1977
HFF600	0 to 16	0 to 16.1	13157	4000*
HFF500	-22 to 22	-23 to 16	11378	697.9
HFF400	-12.5 to 14	-15 to 6	64900	15500*
				*predicted results

Table 1. Table of measured characteristics of 5 types of devices, Triangle from Figure 5 with integrated mirror, and 4 high fill-factor actuators for mirror bonding. HFF600 and HFF400 have not been characterized with bonded mirrors to date.

utilizes a combination of actuators for making micromirrors capable of two-axis scanning as well as pistoning. Symmetry of the design allows both axes to have similar angular rotation and speed, which is highly desirable for applications such as vector or non-raster scanning. Smooth actuation of the device from onset greatly simplifies implementation of control systems.

V. Acknowledgements

The authors would like to thank M. Cohn, R. Roehnelt, and K. Castelino for many useful discussions on the actuator design and micromirror bonding and transfer, as well as C. Keller for many useful discussions and assistance with micromirror transfer.

VI. References

[1] J.-C. Tsai, *et al*, "Analog Micromirror Arrays with Orthogonal Scanning Directions for Wavelength Selective 1xN2 Switches," *Transducers '03*, pp. 1776-1779, Jun. 2003.

[2] Krishnamoorthy, U., *et al,* "Dual-Mode micromirrors for Optical Phased Array Applications", *Transducers'01,* Munich, Germany, June 2001.Germany, Jun. 2001.

[3] V. Milanović, S. Kwon, L. P. Lee, "Monolithic Vertical Combdrive Actuators for Adaptive Optics," *IEEE/LEOS Int. Conference on Optical MEMS*, Switzerland, Aug. 2002.

[4] V. Milanović, "Multilevel-Beam SOI-MEMS Fabrication and Applications," *J. of MEMS,* vol. 13, no. 1, pp. 19-30, Feb. 2004.

[5] P. R. Patterson, *et al*, "A MEMS 2-D Scanner with Bonded Single-Crystalline Honeycomb Micromirror," *Late news, Proc. Solid-State Sensor and Actuator Workshop*, Hilton Head, South Carolina, pp. 17-18, Jun. 2000.

[6] S. Kwon, V. Milanović, L. P. Lee, "A High Aspect Ratio 2D Gimbaled Microscanner with Large Static Rotation," *IEEE/LEOS Int. Conf. on Optical MEMS'02*, Switzerland, Aug. 2002.

[7] H. Schenk, *et al*, "Large Deflection Micromechanical Scanning Mirrors for Linear Scans and Pattern Generation," *IEEE J. of Selected Topics in Quantum Electronics*, vol. 6, no. 5, Sep./Oct. 2000.

[8] T. Brosnihan, et al, "Embedded Interconnect and Electrical Isolation for High-Aspect-Ratio, SOI Inertial Instruments," *1997 Int. Conf. on Solid-State Sensors and Actuators*, Chicago, June 16-19, 1997.

[9] V. Milanović, et al, "Monolithic High Aspect Ratio Two-axis Optical Scanner in SOI," Int. Conf. on Microelectromechanical Systems, MEMS2003, Kyoto, Japan, pp. 255-258, Jan. 2003.

[10] F. Niklaus, S. Haasl and G. Stemme, "Arrays of monocrystalline silicon micromirrors fabricated using CMOS compatible transfer bonding," J. of MEMS , v 12, n 4, Aug. 2003, p 465-469.

[11] U. Srinivasan, et al, "Fluidic self-assembly of micromirrors onto microactuators using capillary forces," IEEE J. of Spec. Topics in Quantum Electronics, vol. 8 (1), pp. 4-11, Jan. 2002.

[12] C. Rembe, *et al*, "Stroboscopic interferometer with variable magnification to measure dynamics in an adaptive-optics micromirror,"
2000 IEEE/LEOS Int. Conf. on Optical MEMS, 21-24 Aug. 2000

[13] http://www.memspi.com

[14] B. Cagdaser, et al, "Capacitive Sense Feedback Control for MEMS Laser Beam Steering Mirrors," *Proc. Solid-State Sensor and Actuator Workshop*, Hilton Head, South Carolina, Jun. 2004.